Spacecraft Attitude Dynamics and Control
De-tumbling and Sun-pointing of a 8U CubeSat in LEO

Aufiero Luca

Course of Spacecraft Attitude Dynamics and Control
Academic Year 2019-2020

Abstract

This project is about the sizing of the Attitude Determination and Control Subsystem of a Sun-pointing 8U CubeSat orbiting around Earth in a circular LEO at an altitude of 600 km. The spacecraft must perform two critical manoeuvers: the de-tumbling and the Sun pointing, using 4 Reaction Wheels and 6 Cold Gas thrusters as actuators, while an Earth Horizon Sensor, a Gyroscope and a Magnetometer are used as sensors. The objective of this report is to present the design strategy that has been developed and implemented within the MATLAB SIMULINK environment, in order to perform a preliminary design and simulation of the control system of such satellite. In the first part of this report, a general description of the architecture of the spacecraft with its ADCS components will be presented; then, the mission requirements will be illustrated, and a brief overview on the mathematical models describing the kinematics and dynamics of the spacecraft will be presented. In the last part it's explained how those mathematical models have been implemented into the MATLAB SIMULINK environment, in order to carry out the necessary simulations, whose results will be presented and discussed.

Abbreviated terms

- A: attitude matrix
- ADCS: Attitude Determination and Control Subsystem
- α: pointing accuracy angle
- ARW: Angular Random Walk
- CG: Cold Gas thrusters
- DCM: Direction Cosine Matrix
- EH: Earth Horizon sensor
- ϵ: error
- h: orbital altitude
- h_r: RW moment of inertia
- IMU: Inertial Measurement Unit
- LEO: Low Earth Orbit
- MS: magnetometer
- $\hat{n}$: normal vector of a surface
- ω: angular velocity
- ψ: equatorial angle
- RAAN: Right Ascension of the Ascending Node
- RRW: Bias Random Walk
- RW: Reaction Wheels
- SRP: Solar Radiation Pressure
- F: force
- G: constant of gravity
- I: moment of inertia
- M: mass

- R: position w.r.t. Sun
- ρ: air density
- S: area
- $\hat{S}_b$: Sun direction in the body frame
- b: magnetic field
- c_D: drag coefficient
- d: disturbance torque
- m: residual magnetic induction
- q: quaternion vector
- r: position w.r.t. Earth
- T: torque
- u: control torque
- v: velocity

Contents

List of Figures

List of Tables

Chapter 1

Introduction

1.1 CubeSat dimensions and structural properties

The satellite considered for this project is the Innovative Solutions In Space 8U CubeSat [1], a miniaturized satellite made up of 8 10 x 10 x 10 cm units. The dimensions of the 8U CubeSat are 226.3 x 226.3 x 227 mm.

Figure 1.1: 8U CubeSat

Considering the mass of the fully loaded CubeSat of 10 kg, we obtain these principal moments of inertia:

I_x	0.1602 $kg * m^2$
I_y	0.1602 $kg * m^2$
I_z	0.1597 $kg * m^2$

Table 1.1: 8U CubeSat principal moments of inertia

The satellite will be modeled as a cuboid with the aforementioned properties. It is assumed that the origin of the body reference frame is centered in the center of gravity of the CubeSat. Another assumption is that the solar panels which could be used to generate the electrical power for the satellite will give a negligible contribution to the mass and the inertia.

1.2 ADCS architecture and components

To perform the required de-tumbling and Sun-pointing manoeuvers the following ADCS components (sensors and actuators) have been chosen: an inertial measurement unit with a gyroscope, a magnetic sensor, an Earth Horizon sensor, 6 cold gas thrusters and 4 reaction wheels.

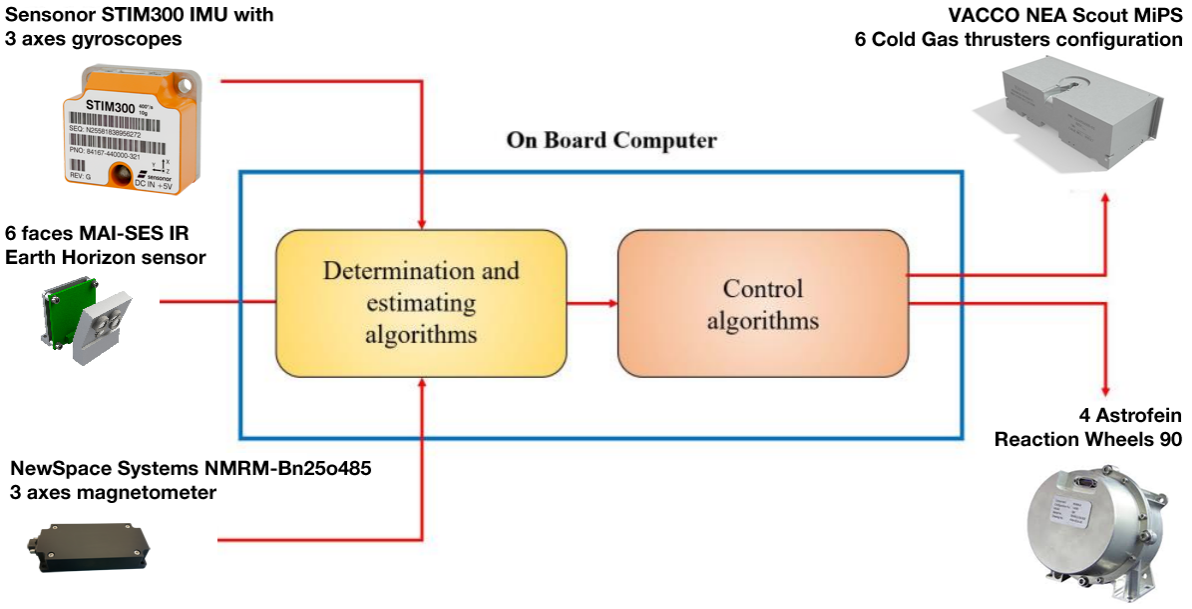

Figure 1.2: ADCS subsystem scheme

1.2.1 IMU and gyroscope

The chosen IMU is a STIM300 by Sensonor [2], wchich contains 3 highly accurate MEMS gyroscopes, 3 high stability accelerometers and 3 inclinometers.

Figure 1.3: STIM300 Inertial Measurement Unit

Mass	55 g
Volume	39 x 45 x 21 mm
RRW	$0.3^o/\text{h}$
ARW	$0.15^o/\sqrt{h}$
Power consuption	1.5 W

Table 1.2: STIM300 IMU properties

1.2.2 Sensors: Earth Horizon Sensor and magnetometer

For the attitude reconstruction, a MAI-SES IR Earth Horizon sensor [3] and a NewSpace Systems NMRM-Bn25o485 magnetometer [4] will be used.

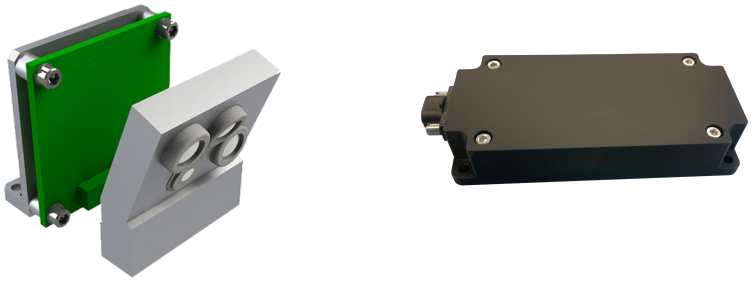

(a) EH (b) MS

Figure 1.4: MAI-SES Earth Horizon Sensor and NewSpace Systems NMRM-Bn25o485 magnetometer

The MAI-SES is a miniature Static Earth Sensor suitable for CubeSats, NanoSats, and larger spacecraft in Low Earth Orbit. The sensor has four thermopile detectors, which view the Earth, Space, and Earth limb and measure the dip angle with respect to the horizon. Two sensor heads mounted orthogonally are required to yield the nadir vector in the body frame.

Mass	33 g
Volume	43 x 32 x 32 mm
Voltage	3.3 V
Field of view coarse resolution	$>$ 1 deg
Coarse field of view	60 deg
Mechanical vibration	$>$ 12 Grms
Fine field of view	7 deg
Field of view fine resolution	0.25 deg

Table 1.3: MAI-SES IR Earth Horizon sensor properties

The NMRM-Bn25o485 magnetometer is ideally mounted outside the spacecraft at the end of a rigid boom and includes low noise, precision processing and analogue-to-digital conversion circuitry, all of which improves the linearity and reduces the drift sensitivity of the sensor head. The integrated processing circuitry and sensor head provide to the mission an accurate and stable magnetic field measurement at low power consumption. The design of the tri-axial magnetometer uses Anisotropic Magneto-Resistive (AMR) sensors which are co-located with offset compensating circuitry. The offset compensating circuitry nulls the characteristic offset voltage of the AMR sensor and enhances the sensors performance. The sensor provides x, y and z axes magnetic field component measurements, as well as a sensor temperature measurement which is used for the temperature compensation of the magnetic field measurement.

Maximum mass	85 g
Volume	99 x 43 x 17 mm
Voltage	5 V
Radiation tolerance	10 krad
Magnetic field range	min: -60000 nT, max: 60000 nT
Maximum power	$>$ 12 750 mW
Maximum update rate	18 Hz
Operating temperature	min: -25^{o}C, max: 70^{o}C

Table 1.4: NMRM-Bn25o485 magnetometer properties

1.2.3 Actuators: cold gas thrusters and reaction wheels

For the actuation, six cold gas thrusters in the VACCO NEA Scout MiPS configuration [5] will be used for the de-tumbling. The VACCO NEA Scout MiPS is approximately 2U in volume and uses six 25 mN cold gas thrusters to develop 500 N-sec of total impulse that can provide 37 m/s of delta-V for a 14 kg CubeSat. Each thruster independently operates to perform both delta-V and ACS maneuvers through an integrated microprocessor controller.

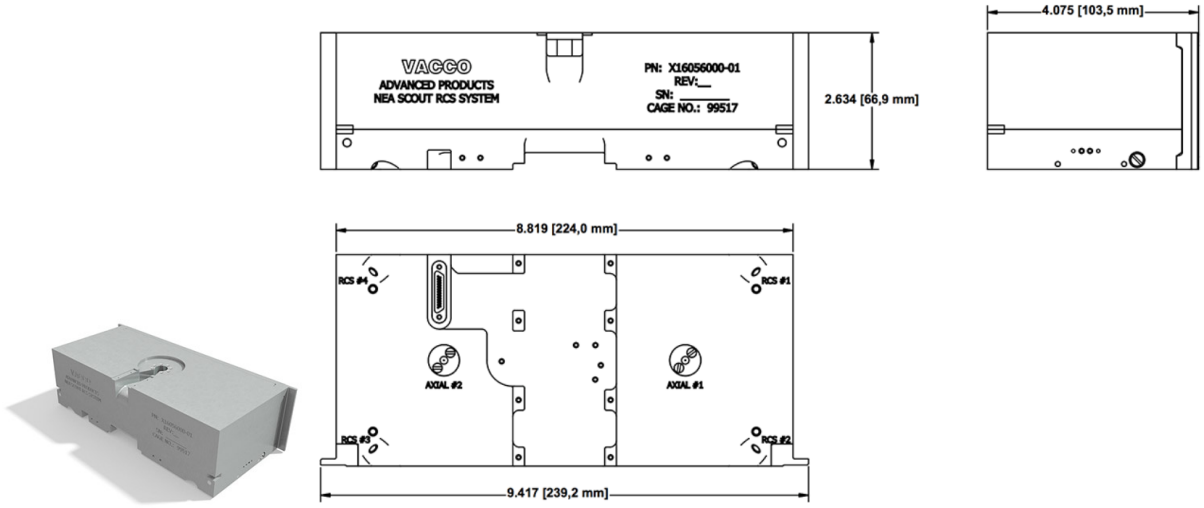

(a) structure (b) scheme

Figure 1.5: VACCO NEA Scout MiPS 6 CG configuration

Propellant	R236fa
MDP	6.89 Bar (100 psia)
Proof pressure	10.34 Bar (150 psia)
Burst pressure	13.79 Bar (200 psia)
Maximum internal leakage	0.5 scch R-236fa
Maximum external leakage	$1.0 * 10^{-6}$ sccs GHe
Operating temperature	min: -10^{o}C, max: 55^{o}C
Non-operating temperature	min: -24^{o}C, max: 55^{o}C
Total impulse at 10^{o}C	500 N-s
Dry mass	1.263 kg Max
Wet Mass 95% Fill at 10^{o}C	2.540 kg Max
Operating voltage	9.0-12.6 V
Standby power	1.1 W Max
Warmup power	$1.0 * 10^{-6}$ 55 W Max
Thruster Operating Power (4 thrusters)	9 W Max
Data interface	RS-422

Table 1.5: VACCO NEA Scout MiPS 6 CG properties

Reaction wheels have been designated as main momentum exchange device and are used for pointing and slew manoeuvre. For a 3-axis stabilization 3 RW mounted on three different axes are required, and a fourth one which can work in each of the 3 axes is mounted as a backup. The hardware selected is Reaction Wheel 90 by Astrofein [6]. The RW 90 is a flight proven smart reaction wheel for small and micro satellites with integrated wheel drive electronics, different operation modes for speed and acceleration using model based controllers, high torque and speed stability (low noise), internal compensation of friction and time delays, housekeeping, and protective and monitoring mechanisms.

Figure 1.6: Astrofein Reaction Wheel 90

Maximum mass	0.9 kg
Volume	103 x 101 x 80 mm
Maximum power consumption	15 W
Maximum torque	0.015 Nm
Angular speed	6000 rpm
Max angular speed	7800 rpm
Operating T	-20^{o}C to 50^{o}C
Voltage	18 V to 34 V
Moment of inertia	4.2 e-4 kg m^2
Angular momentum storage	0.34 Nms

Table 1.6: Astrofein Reaction Wheel 90 properties

1.3 Mission parameters and requirements

Our CubeSat will fly on a circular LEO with the following orbital parameters

Semi-major axis	$a = 6371 + 600\ km$
Eccentricity	$e \simeq 0$
Inclination	$i = 0^o$
Argument of perigee	$\omega = 0$
RAAN	$\Omega = 0$

Table 1.7: orbital parameters of the spacecraft around the Earth

When it's released from the fairing, the CubeSat has a tumbling motion with random initial angular rates (we assume thy are 0.1 rad/s around the 3 axes). A deeper analysis could consider the specific launcher: by looking at its manual it's possible to find the actual estimated angular rates at which the spacecraft will rotate after being injected into orbit. The detumbling manoeuver will be performed by the cold gas thrusters, that will bring the spacecraft to rest, that is angular rates almost equal to 0. After the de-tumbling, the Sun pointing manoeuver will be performed by the 4 reaction wheels.

1.4 Disturbance torques

There are two types of disturbance torques which will affect the spacecraft operations. The first ones are related to the orbital environment: aerodynamic drag, solar radiation pressure, gravity gradient and Earth's magnetic field. The second ones are due to internal disturbances: propellant slosh, flexible parts and eventual parasite torques arising after thrust misalignment. In this report only the first family of disturbances are considered and modeled.

1.4.1 Aerodynamic torque

Upper atmosphere particles collide with the CubeSat, exerting force on its lateral surfaces; due to the offset between the centre of pressure and the centre of gravity, a net torque about the latter arises. Such offset has been considered to be the 10% of the sides of the spacecraft. The force due to air drag is computed in this way:

$$\vec{F}_{drag} = -\frac{1}{2} * S_{cross,i} * c_D * \rho * \|\vec{v}_{rel}\|^2 * \frac{\vec{v}_{rel}}{\|\vec{v}_{rel}\|^2} \tag{1.1}$$

Where ρ is the atmospheric density, computed according to the Exponential Atmospheric Model, $S_{cross,i}$ is the i-th surface of the spacecraft:

$$S_{cross,i} = S_i * \hat{n}_i \frac{\vec{v}_{rel}}{\|\vec{v}_{rel}\|^2} \quad if \quad \hat{n}_i \frac{\vec{v}_{rel}}{\|\vec{v}_{rel}\|^2} \geq 1 \tag{1.2}$$

otherwise $S_{cross,i}$ it's equal to 0. The relative velocity is the one between the spacecraft and Earth's rotating atmosphere. The drag coefficient has been assumed to be $c_D = 2.2$, a good approximation for a flat plate. In LEO air drag torque is the most relevant disturbance torque. In this case it generates a disturbance in the order of 10^{-4} Nm.

1.4.2 Gravity gradient torque

The gravity gradient is the torque exerted by Earth's gravity field when the pointing axis, that is the first column of $A_{B/N}$, is not exactly directed towards Earth's centre. It is

possible to quantify the misalignment by taking the first column of $A_{B/L}$. The intensity of this disturbance depends also on the distance of the spacecraft from the Earth.

$$\begin{cases} T_{gg,1} = \frac{3Gm_e}{r^3}(I_z - I_y)c_3c_2 \\ T_{gg,2} = \frac{3Gm_e}{r^3}(I_x - I_z)c_1c_3 \\ T_{gg,3} = \frac{3Gm_e}{r^3}(I_y - I_x)c_2c_1 \end{cases} \tag{1.3}$$

where

$$\begin{pmatrix} c_1 \\ c_2 \\ c_3 \end{pmatrix} = A_{B/L} \begin{pmatrix} 1 \\ 0 \\ 0 \end{pmatrix} \tag{1.4}$$

In the considered orbit, for the 8U CubeSat, gravity gradient torque generates a very low disturbance, in the order of 10^{-12} Nm.

1.4.3 Magnetic field torque

This disturbance is the result of Earth's magnetic field on the micro satellite. Any satellite has a residual magnetic induction (which can be approximated as equal to 0.1 Am^2 on each axis), due to the electronics on board; this will interact with the magnetic field, modeled by means of a basic dipole model, generating a torque.

$$T_{MF} = m_{res} \times B \tag{1.5}$$

In the considered orbit magnetic field torque generates a disturbance in the order of 10^{-6} Nm.

1.4.4 Solar Radiation Pressure

The Solar radiation pressure disturbance is the result of the impact of the photons emitted by the Sun on the spacecraft. Since the centre of the solar radiation pressure has an offset with respect to the centre of mass, this pressure generates a torque, similarly to what happens with air drag. The radiation force considers absorption, reflection and diffusion over the surface and for a flat panel can be written as:

$$\begin{cases} \vec{F}_{SRP,i} = P_{SRP}S_b(\hat{S}_b \bullet \hat{n}_i)[(1-\rho_s)\hat{S}_b + (2\rho_s(\hat{S}_b \bullet \hat{n}_i) + \frac{2}{3}\rho_d)\hat{n}_i] \quad if \quad \hat{S}_b \bullet \hat{n}_i \geq 0 \\ \vec{F}_{SRP,i} = \vec{0} \quad if \quad \hat{S}_b \bullet \hat{n}_i < 0 \end{cases} \tag{1.6}$$

The torque induced by this force is equal to

$$T_{SRP} = \sum_{i}^{Nfaces} b_i \times \vec{F}_{SRP,i} \tag{1.7}$$

The ρ parameters represent the specular and diffusive reflectivity of a body; we used typical values of $\rho_d = 0.1$ and $\rho_s = 0.5$. To find $\hat{S}_b$, the first step is to compute the position of the satellite w.r.t. the Sun:

$$\vec{R}_{S/C} = \vec{R}_E + A_{S/N}\vec{r}_{S/C} \tag{1.8}$$

The rotation matrix $A_{S/N}$ considers the fact that the Ecliptic plane is inclined with respect to the Equatorial plane of an angle $\psi = 23.45^o$. The rotation is performed around the y axis of the Earth's inertial frame, so that both Spacecraft and Earth's position are in the Sun reference frame and can be added. To obtain $\hat{S}_b$, the vector $\vec{R}_{S/C}$ must be expressed in the body reference frame:

$$\vec{r}_{SUN} = A_{B/N} A_{N/S} \vec{R}_{S/C} \tag{1.9}$$

The matrix $A_{N/S}$ rotates back of the angle ψ and, multiplied by $A_{B/N}$, it expresses the position of the Sun in the body reference frame. $\vec{r}_{SUN}$ is the position of the Sun in the body frame, so that the versor associated with $\vec{r}_{SUN}$ is the Sun direction we wanted: $\hat{S}_b$. In the considered orbit SRP torque generates a disturbance in the order of 10^{-7} Nm. During the LEO orbiting, sometimes the spacecraft is shadowed from sunlight by the Earth, and in this situation there is no torque induced by SRP. We assume the CubeSat is always hit by sunlight, to consider the worst case in which we always have SRP disturbance torques. Anyway, in this case, the torque induced by SRP is almost irrelevant with respect to air drag torque.

1.4.5 Overall disturbance torque

Summing all the previously calculated disturbance torques we obtain the overall disturbance torques on the spacecraft during the two manoeuvers we have to perform: de-tumbling and pointing. The most influential disturbance torque in the considered orbit is the aerodynamic torque.

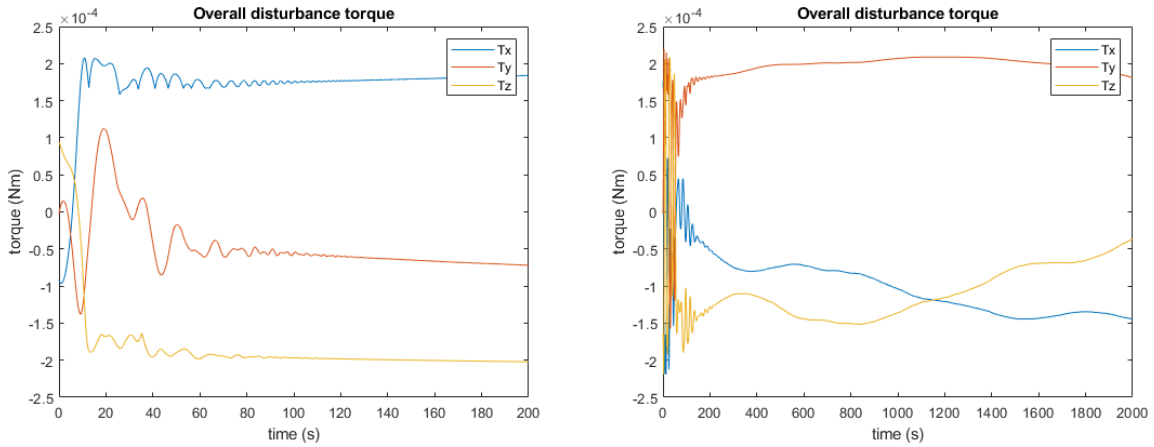

(a) De-tumbling

(b) Pointing

Figure 1.7: Disturbance torques

Chapter 2

ADCS design

In this section there will be a description of the mathematical models used to represent the behaviour of the spacecraft, of the actuators and of the attitude determination systems.

2.1 Dynamics

Euler equations describe the evolution of the angular velocities in the body frame: $\vec{\omega}_{B/N}$, including moments of inertia, disturbances and control torques. The integration requires the definition of the initial conditions, assumed to be the initial tumbling spin rate of 0.1 rad/s around each axis.

$$\begin{cases} \dot{\omega}_{B/N,1} = \frac{I_2 - I_3}{I_1}\omega_2\omega_3 + \frac{T_{dist,1}}{I_1} + \frac{T_{contr,1}}{I_1} \\ \dot{\omega}_{B/N,2} = \frac{I_3 - I_1}{I_2}\omega_1\omega_3 + \frac{T_{dist,2}}{I_2} + \frac{T_{contr,2}}{I_2} \\ \dot{\omega}_{B/N,3} = \frac{I_1 - I_2}{I_3}\omega_2\omega_1 + \frac{T_{dist,3}}{I_3} + \frac{T_{contr,3}}{I_3} \end{cases} \tag{2.1}$$

The output vector $\vec{\omega}_{B/N}$ represents the angular velocity of the body fixed frame with respect to the inertial frame.

2.2 Kinematics

The quaternions are the kinematic representation adopted in this project, thanks to their higher computational efficiency with respect to DCM (4 components instead of 9 to be integrated) and the absence of singularities in opposition with Euler angles and Rodrigues parameters.

$$\begin{pmatrix} \dot{q}_1 \\ \dot{q}_2 \\ \dot{q}_3 \\ \dot{q}_4 \end{pmatrix} = \frac{1}{2}\begin{bmatrix} 0 & \omega_3 & -\omega_2 & \omega_1 \\ -\omega_3 & 0 & \omega_1 & \omega_2 \\ \omega_2 & -\omega_1 & 0 & \omega_3 \\ \omega_3 & \omega_2 & -\omega_1 & 0 \end{bmatrix}\begin{pmatrix} q_1 \\ q_2 \\ q_3 \\ q_4 \end{pmatrix} \tag{2.2}$$

Then it's possible to find the attitude matrix $A_{B/N}$ with the quaternions:

$$A_{B/N} = \frac{1}{2}\begin{bmatrix} q_1^2 - q_2^2 - q_3^2 + q_4^2 & 2(q_1q_2 + q_3q_4) & 2(q_1q_3 - q_2q_4) \\ 2(q_1q_2 - q_3q_4) & -q_1^2 + q_2^2 - q_3^2 + q_4^2 & 2(q_2q_3 + q_1q_4) \\ 2(q_1q_3 + q_2q_4) & 2(q_2q_3 - q_1q_4) & -q_1^2 - q_2^2 + q_3^2 + q_4^2 \end{bmatrix} \tag{2.3}$$

2.3 Reference attitude

We have to compute the desired attitude $A_{L/N}$, which is an orthonormal right reference frame with the first axis directed towards the Sun. The pointing will be successful if the difference between $A_{B/N}$ and $A_{L/N}$ tends to zero, which means $A_{B/N}A_{L/N}^T = I$. As the distance between the spacecraft and the Earth is much lower than the distance between the Earth and the Sun, we assume that the CubeSat has the same orbit of the Earth around the Sun, without considering its rotation around the Earth; this orbit has the following orbital parameters:

Semi-major axis	$149.6 * 10^6\ km$
Eccentricity	0.0167
Inclination	$i = 0^o$
Argument of perigee	$\omega = 0$
RAAN	$\Omega = 0$

Table 2.1: orbital parameters of the Earth around the Sun

Those parameters are converted in Cartesian initial conditions and used for the integration of the orbital dynamics, by means of Newton's Gravitational Law. The outputs of this computation are the position ($\vec{r}$) and velocity ($\vec{v}$) vectors of the Earth, and so of the spacecraft, with respect to the Sun; these are used to compute the $A_{L/N}$ matrix:

$$\begin{cases} \hat{r}_1 = \frac{\vec{r}}{\|\vec{r}\|} \\ \hat{r}_3 = \frac{\hat{r}_1 \times \vec{v}}{\|\hat{r}_1 \times \vec{v}\|} \\ \hat{r}_2 = \hat{r}_3 \times \hat{r}_1 \end{cases} \tag{2.4}$$

$$A_{L/N} = \begin{bmatrix} \hat{r}_1^T & \hat{r}_2^T & \hat{r}_3^T \end{bmatrix} \tag{2.5}$$

2.4 Attitude determination

Attitude determination is very important to perform with success the de-tumbling and pointing manoeuvers required for this mission. In a real situation, the attitude matrix and the rotational dynamic of a spacecraft aren't known, so they have to be reconstructed by on board sensors, that in this case consist in a gyroscope, an Earth horizon sensor and a magnetometer.

2.4.1 Gyroscope

Gyroscopes are mechanical devices used to measure angular velocities on one axis. The STIM300 IMU we use contains 3 gyroscopes, so it can measure the angular rates around each axis. The measured angular velocities are given by:

$$\omega_{measured} = \omega + n + b \tag{2.6}$$

where n and b are random noises, modeled as Gaussian white noise with zero mean and standard deviation given by the following equations:

$$\begin{cases} \mu_n = 0 \\ \sigma_n = ARW * \sqrt{f} \end{cases} \tag{2.7}$$

$$\begin{cases} \mu_b = 0 \\ \sigma_b = RRW * \sqrt{f} \end{cases} \tag{2.8}$$

ARW is the Angular Random Walk, attributed to thermo-mechanical noise, RRW is the Bias Random Walk, that is the bias due to electronic noise. Their values are taken from the datasheet of the sensor. In order to mitigate the effect of these noises, a low pass filter is implemented right after the gyroscope output.

2.4.2 Earth horizon sensor and magnetometer

The Earth horizons sensor and the magnetometer are modeled considering a random error of maximum value equal to the accuracy of the sensors. Each measurement the two sensors make is affected by an angle error that depends on the sensor accuracy. For a magnetometer the accuracy is $\psi = \theta = \phi = 300\ arcmin = 5\ deg$ while for the EH sensor the accuracy is $\psi = \theta = \phi = 6\ arcmin = 0.1\ deg$. In theory there should be 3 angular errors, one for each axis, but we assume they are all equal. With these errors we build the error matrix:

$$A_\epsilon = \begin{pmatrix} cos(\psi)cos(\theta) & cos(\psi)sin(\theta)sin(\phi)+ & -cos(\psi)sin(\theta)cos(\phi)+ \\ & +sin(\psi)cos(\phi) & +sin(\psi)sin(\phi) \\ -sin(\psi)cos(\theta) & -sin(\psi)sin(\theta)sin(\phi)+ & sin(\psi)sin(\theta)cos(\phi)+ \\ & +cos(\psi)cos(\phi) & +cos(\psi)sin(\phi) \\ sin(\theta) & -cos(\theta)sin(\phi) & cos(\theta)cos(\phi) \end{pmatrix} \tag{2.9}$$

Using the on board models of the magnetic field and of the direction vector of the Earth with respect to the spacecraft (subscript N) we can compute the values obtained by the sensors (subscript B):

$$h_B = A_\epsilon A_{B/N} h_N \tag{2.10}$$

$$b_B = A_\epsilon A_{B/N} b_N \tag{2.11}$$

2.4.3 Determination algorithm

The two different measures we have allow us to use a static method, instead of a dynamic one. The best determination algorithm we can use if the measurements from two different sensors are available is the TRIAD method. Two orthogonal frames can be built from sensors measurements and the inertial directions coming from the reference models:

$$V_B = \begin{bmatrix} h_B & \frac{h_B \times b_B}{\|h_B \times b_B\|} & h_B \times \frac{h_B \times b_B}{\|h_B \times b_B\|} \end{bmatrix} \tag{2.12}$$

$$V_N = \begin{bmatrix} h_N & \frac{h_N \times b_N}{\|h_N \times b_N\|} & h_N \times \frac{h_N \times b_N}{\|h_N \times b_N\|} \end{bmatrix} \tag{2.13}$$

Then we can determine the attitude matrix:

$$A_{B/N} = V_B V_N^T \tag{2.14}$$

2.4.4 Alternative determination algortihms

With the measurements obtained by two different sensors we could use other attitude determination algorithms, like q method, QUEST method or Single Value Decomposition (SVD). For example, using the QUEST method, we obtain very similar results with respect to the TRIAD method, spending more or less the same computational time; the slew manoeuver is completed after the same amount of time, but in the end we have a slightly higher pointing error, so with the TRIAD method we have a more accurate pointing manoeuver. The comparison graphs between the two methods are shown in the section 3.2.

2.5 Control

The two required manoeuvers will be performed thanks to two different kind of actuators: cold gas thrusters for de-tumbling and reaction wheels for pointing.

2.5.1 De-tumbling control

As it's performed by cold gas thrusters, the de-tumbling is based on a simple Bang-Bang type controller, exploiting the measured angular velocities from the gyroscope $\vec{\omega}_{measured}$, and seeking asymptotic stability by means of the following ideal control law:

$$\vec{u}_{ideal} = -T_{max} * sign(\vec{\omega}_{measured}) \tag{2.15}$$

To avoid chattering the thrusters are switched on only if $\vec{\omega}_{measured}$ goes above a certain threshold. In the VACCO's NEA SCOUT 6 cold gas thrusters configuration we have chosen, 2 thrusters are fixed in the +z direction for major orbital change or adjustment manoeuvers. The other 4 thrusters can be moved and are used for attitude control. We assume to fix them in the $\alpha = 15^o$ configuration, so that we have a complete 3 axes controllability with 4 fixed cold gas thrusters. With this configuration we obtain:

$$T_{max} = \begin{pmatrix} 2lFsin(\alpha) \\ 2lFcos(\alpha) \\ 2(x_1 Fcos(\alpha) - x_2 Fsin(\alpha)) \end{pmatrix} \tag{2.16}$$

with l equal to the distance between the thrusters and the CubeSat gravity center in the z axis, x_1 equal to half of the distance between the thrusters in the y axis, and x_2 equal to half of the distance between the thrusters in the x axis. Other two parameters, taken from the datasheet of the thrusters, have been modeled: the MIB, by means of the "zero order hold" block, and a rate limiter to simulate the fact that the system does not respond instantaneously, but there are characteristic rise (10 ms) and fall (50 ms) times to be taken into account.

2.5.2 Pointing ideal control

To compute the ideal control action the computation of an error, in terms of angular velocities and attitude, is required. The attitude error, expressed as the quaternion error, can be computed finding the attitude error in terms of DCM:

$$A_{err} = A_{B/N} * A_{L/N}^{T} \tag{2.17}$$

and then transforming it into the quaternion error q_{err}. The angular velocity error ω_{err} is equal to the difference between the angular velocity measured by the gyroscope and the desired one we set equal to 0. When using the quaternion error, the pointing control law is based on a function of the scalar component of the quaternion error, $H(q_{4e})$, selected to satisfy Lyapunov stability conditions and to avoid possible unwinding phenomena. In this study, the following H function has been adopted:

$$H(q_{4e}) = 1 - q_{4e}^{2} \tag{2.18}$$

$$\frac{dH(q_{4e})}{dq_{4e}} = -2q_{4e} \tag{2.19}$$

The pointing ideal control law is:

$$\vec{u}_{ideal} = \vec{\omega}_{err} \times J\vec{\omega}_{err} - k_1\vec{\omega}_{err} + k_2\frac{dH(q_{4e})}{dq_{4e}}\vec{q}_{err} \tag{2.20}$$

The gain k_1 has been chosen with a trial and error method, while k_2 has been optimized through the equation:

$$k_2 = \frac{k_1^2}{2} \tag{2.21}$$

2.5.3 Pointing RW control

The 4 RW configuration leads to a disposition matrix of

$$A = \begin{pmatrix} 1 & 0 & 0 & 1/\sqrt{3} \\ 0 & 1 & 0 & 1/\sqrt{3} \\ 0 & 0 & 1 & 1/\sqrt{3} \end{pmatrix} \tag{2.22}$$

From the ideal control we obtain the real reaction wheel control action:

$$\dot{\vec{h}}_r = -A^{*}(\vec{u}_{ideal} + \vec{\omega}_{B/N} \times A\vec{h}_r) \tag{2.23}$$

where A^{*} is the pseudoinverse matrix of A and $\vec{h}_r = \vec{I}_{RW}\vec{\omega}_{RW}$ is the momentum of the reaction wheel;

$$\vec{u}_{real} = -A\dot{\vec{h}}_r + A\vec{h}_r \times \vec{\omega}_{B/N} \tag{2.24}$$

The physical model of the RW includes saturation limit for the maximum reaction wheel momentum (0.34 Nms) and the maximum available torque (0.015 Nm).

Chapter 3

Results and conclusions

In this section, the results coming from the simulations of the two manoeuvers required for accomplishing the mission, de-tumbling and Sun pointing, are presented and discussed.

3.1 De-tumbling

The aim of the de-tumbling manoeuver is to reduce the angular velocity from the starting one immediately after the release from the fairing to approximately zero. The initial tumbling angular rates at release (we assume they are 0.1 rad/s around each axis; we also tested the simulation with different initial conditions, and we verified it's robust to initial conditions variations) are measured thanks to the IMU (gyroscope), and they are the input of the bang-bang control action of the cold gas thrusters, that reduce the angular rates to approximately zero.

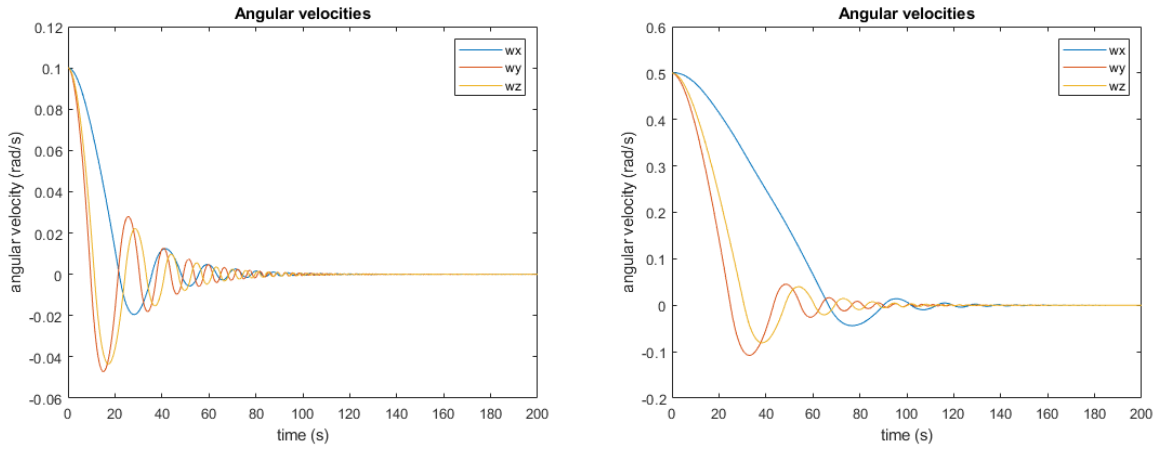

(a) Assumed initial conditions

(b) Different initial conditions to verify robustness

Figure 3.1: De-tumbling angular velocities

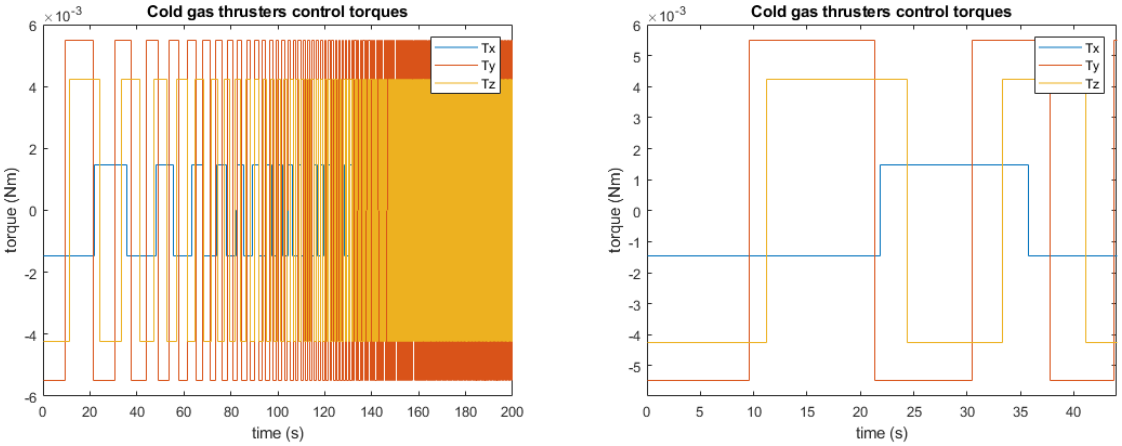

(a) Total simulation duration

(b) First 45 seconds zoomed

Figure 3.2: Cold gas thrusters control torques

As we can see from the results the de-tumbling manoeuver can be considered complete after 130 s. The angular velocity of the spacecraft will never be exactly zero because of the environmental disturbances and the anti-chattering strategy used in the CG thrusters model, but a value in the order of 10^{-5} rad/s is acceptable. From the cold gas thrusters control torques graph we can see that when the angular velocity is close to zero, the cold gas thrusters make continuous micro-corrections to compensate the disturbance torques. For this reason the de-tumbling manoeuver must be stopped when the angular velocities are close to 0, and not exactly 0. From the zoomed image of the cold gas thrusters control torques the bang-bang nature of this kind of control is clear.

3.2 Pointing

After de-tumbling, the CubeSat has the desired angular velocity of approximately zero, but it's pointing towards a random direction, while the objective of the mission is to point towards the Sun. So we must perform a slew manoeuver, to bring the spacecraft from the rest state reached after the de-tumbling to the desired Sun-pointing rest state. This manoeuver is performed by the reaction wheels, with the aim of reducing the attitude error between the desired attitude and the CubeSat one (obtained thanks to the magnetometer and the Earth horizon sensor) to 0. Then the sensors and the reaction wheels must keep determining and controlling the attitude to maintain the Sun-pointing throughout the whole duration of the mission.

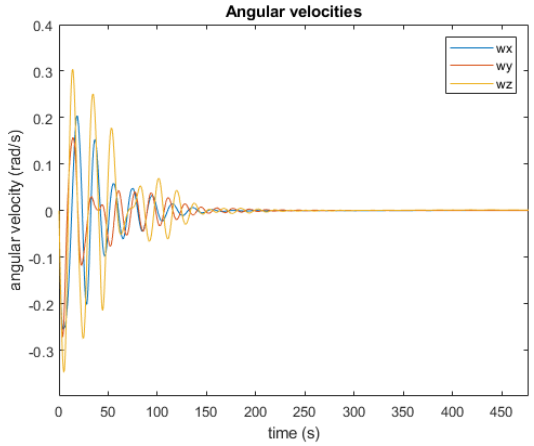

(a) TRIAD method

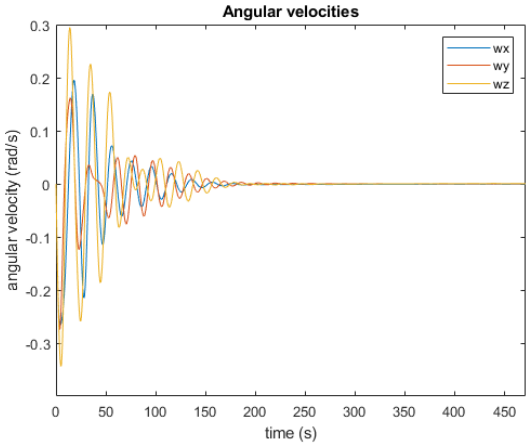

(b) QUEST method

Figure 3.3: Slew and pointing angular velocities

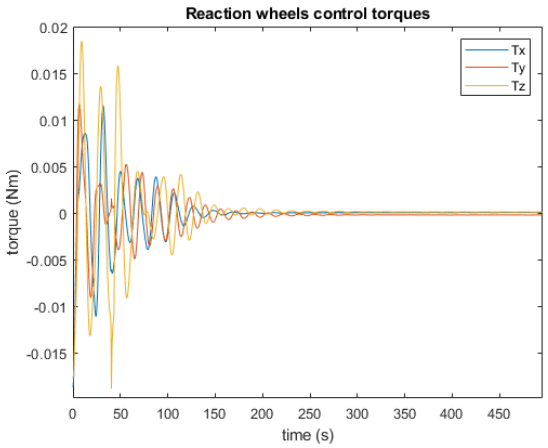

(a) First 500 seconds

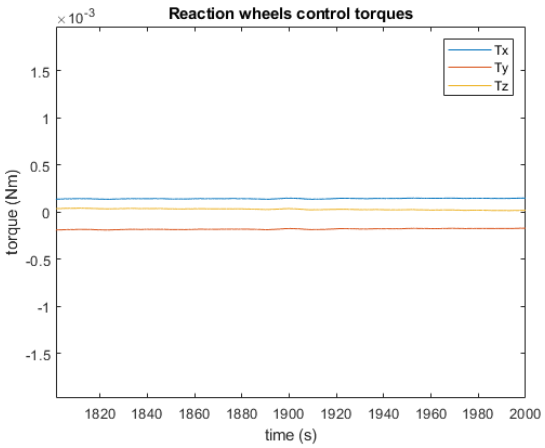

(b) After 2000 seconds

Figure 3.4: Reaction wheels control torques

As we can see from the results the slew manouever can be considered complete after 300 s, when the spacecraft is pointing towards the Sun and its angular velocities are back to approximately 0. But, as it's clearly shown in figure 3.4 b, the reaction wheels constantly keep working to maintain the Sun-pointing: their control torques are small to balance the disturbance torques and the CubeSat rotation around the Sun, but they never go to 0.

3.2.1 Attitude estimation error and pointing error

To ensure that the spacecraft reaches the right Sun-pointing attitude and keeps it in time we can plot the attitude estimation error and the pointing error. To measure the attitude estimation error we use the quaternion error. The final equilibrium condition that should be reached after a slew manoeuver is $\vec{q_0} = \begin{bmatrix} 0 & 0 & 0 & 1 \end{bmatrix}^T$. As it can be seen in the following graph, the quaternion error components converge to the desired ones,

suggesting that after 300 s the reached attitude is almost equal to the desired one, and also beyond 300 s the attitude remains almost always correct .

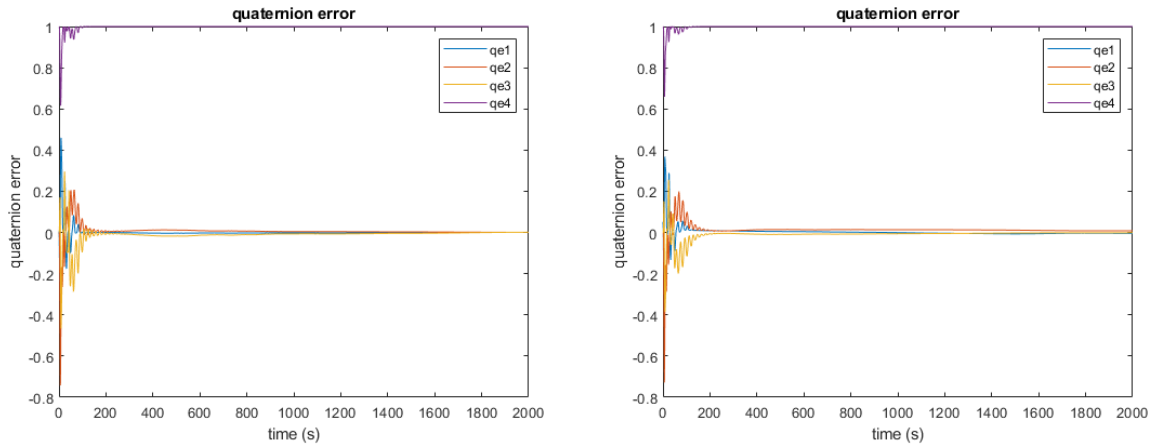

(a) TRIAD method (b) QUEST method

Figure 3.5: Attitude estimation error (quaternion error)

Finally we can plot the pointing accuracy. In the following plots, which are representative of the slew and pointing phases, it is possible to see the trend of the pointing angle error. Beyond 300 s the pointing error constantly remains below 2.5 degrees, and after 1600 s it goes below 0.5 degrees, which is a very good value.

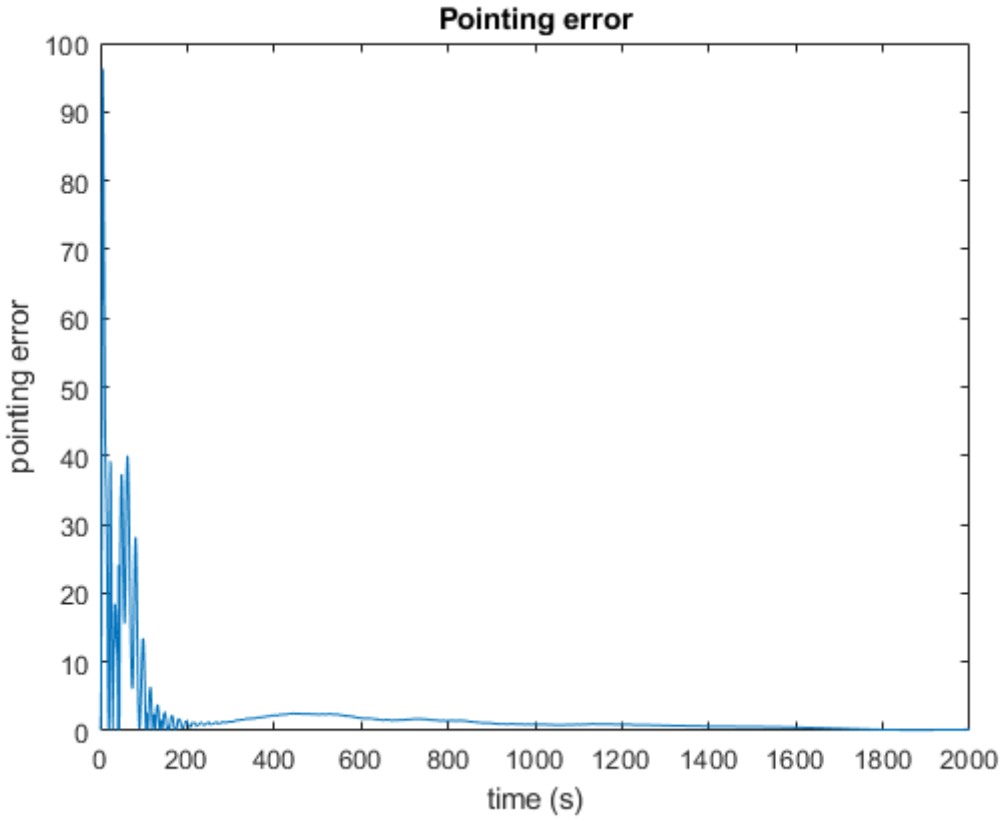

Figure 3.6: Pointing error

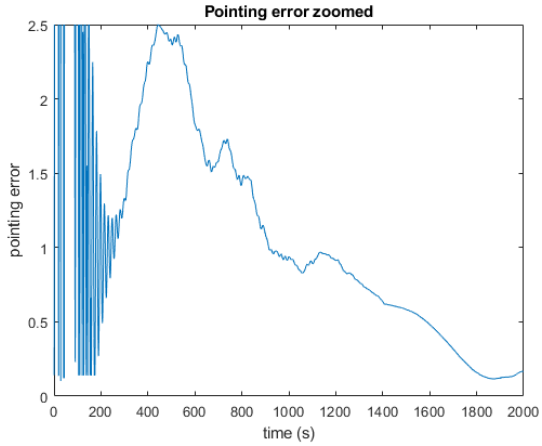

(a) TRIAD method

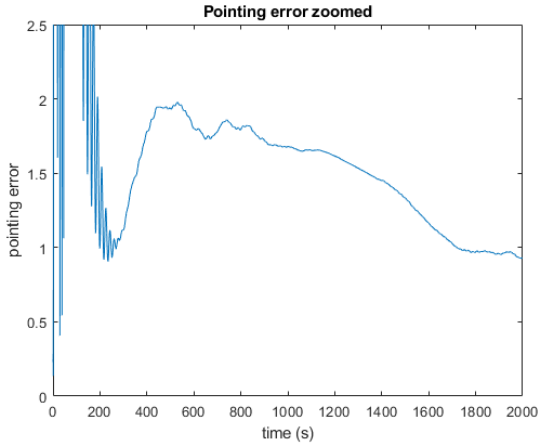

(b) QUEST method

Figure 3.7: Zoomed pointing error

Bibliography

[1] Innovative Solutions In Space: 8-Unit CubeSat structure

[2] Sensonor: STIM300 IMU

[3] CubeSatShop: MAI-SES IR Earth Sensor

[4] SatSearch: NMRM-Bn25o485 magnetometer

[5] CubeSat Propulsion: VACCO's NEA SCOUT cold gas Micro Propulsion System (MiPS)

[6] Astrofein: Reaction Wheel RW 90